The Myokinetic Control Interface: How Many Magnets Can be Implanted in an Amputated Forearm? Evidence From a Simulated Environment

Stefano Milici, Marta Gherardini, *Graduate Student Member, IEEE*, Francesco Clemente, Federico Masiero, Paolo Sassu, and Christian Cipriani, *Senior Member, IEEE*

***Abstract*— We recently introduced the concept of a new human-machine interface (the *myokinetic control interface*) to control hand prostheses. The interface tracks muscle contractions via permanent magnets implanted in the muscles and magnetic field sensors hosted in the prosthetic socket. Previously we showed the feasibility of localizing several magnets in non-realistic workspaces. Here, aided by a 3D CAD model of the forearm, we computed the localization accuracy simulated for three different below-elbow amputation levels, following general guidelines identified in early work. To this aim we first identified the number of magnets that could fit and be tracked in a proximal (T1), middle (T2) and distal (T3) representative amputation, starting from 18, 20 and 23 eligible muscles, respectively. Then we ran a localization algorithm to estimate the poses of the magnets based on the sensor readings. A sensor selection strategy (from an initial grid of 840 sensors) was also implemented to optimize the computational cost of the localization process. Results showed that the localizer was able to accurately track up to 11 (T1), 13 (T2) and 19 (T3) magnetic markers (MMs) with an array of 154, 205 and 260 sensors, respectively. Localization errors lower than 7% the trajectory travelled by the magnets during muscle contraction were always achieved. This work not only answers the question: "how many magnets could be implanted in a forearm and successfully tracked with a the myokinetic control approach?", but also provides interesting insights for a wide range of bioengineering applications exploiting magnetic tracking.**

***Index Terms*— Magnetic tracking, myokinetic interface, upper limb prosthetics, human-machine interface, magnetic field.**

I. Introduction

AN UPPER extremity amputation is an event that profoundly affects the quality of life in several aspects, limiting the individual in performing working and daily living activities. Commercially available artificial hands and arms are often controlled through surface EMG electrodes that record the electrical activity generated by the residual muscles when contracting. Often, this approach suffers the lack of accessible independent control sources, and its performance is thus limited in the case of multi-articulated prostheses [1]. In the last years, different solutions have been proposed to overcome this limitation and increase the number of degrees of freedom (DoFs) that can be controlled independently. New technologies like wireless implantable myoelectric sensors (IMES) [2], [3] or epimysial electrodes wired through osseointegrated implants [4], [5], enabled direct interfacing with the physiological structures (muscles and nerves) involved in the motor control, when still intact. For those cases where the muscles were eradicated by the amputation, new surgical procedures, like targeted muscle reinnervation [6] or regenerative peripheral nerve interfaces [7], allowed to increase the number of independent control sites redirecting the nerve residual limbs to new recipient muscles. Despite the exciting recent advances of these promising approaches [8], [9], a human-machine interface enabling physiological control over a large number of DoFs has to be demonstrated yet.

Our group recently proposed a new concept of human-machine interface for the control of artificial limbs that takes advantage of magnetic tracking, termed *myokinetic control interface* [10]. The idea is to implant multiple permanent magnets (magnetic markers – MMs) into the residual muscles of an individual with upper limb amputation, track their movements using magnetic sensors hosted in the socket, and use these signals as control inputs in a prosthesis, e.g. a hand. Notably, localizing the implanted magnets is equivalent to measure the contraction/elongation of the muscle they are implanted in, as the magnets move with it. This approach could potentially allow to physiologically control multiple, independent DoFs in the prosthesis by exploiting simple passive implants.

Such a system comprises a localizer that retrieves the *pose* of the MMs (i.e., their position and orientation) using multiple recordings of the magnetic field acquired through magnetic field sensors, i.e., solving the inverse problem of magnetostatics [11]. Most of the magnetic tracking systems proposed so far reconstruct the pose of a single marker using

Manuscript received May 26, 2020; revised September 7, 2020; accepted September 13, 2020. Date of publication September 21, 2020; date of current version November 6, 2020. This work was supported by the European Research Council through the bidirectional MyoKinetic implanted Interface for Natural Control of Artificial limbs (MYKI) Project under Grant ERC-2015-StG and Grant 679820. *(Corresponding author: Christian Cipriani.)*

Stefano Milici, Marta Gherardini, Francesco Clemente, Federico Masiero, and Christian Cipriani are with the Biorobotics Institute, Scuola Superiore Sant'Anna, 56127 Pisa, Italy, and also with the Department of Excellence in Robotics and AI, Scuola Superiore Sant'Anna, 56127 Pisa, Italy (e-mail: christian.cipriani@santannapisa.it).

Paolo Sassu is with the Department of Hand Surgery, Sahlgrenska University Hospital, 413 45 Gothenburg, Sweden.

Digital Object Identifier 10.1109/TNSRE.2020.3024960

an appropriate number of sensors. A few exceptions to single marker systems are the trackers developed by Yang *et al.* [12], Taylor *et al.* [13] and Tarantino *et al.* [14] that considered the pose of three (15 unknowns), four (20 unknowns) or seven (35 unknowns) markers.

In particular, in [14] we investigated the viability and the performance of a multi-magnet tracking system in a workspace/volume resembling the bulk dimensions of the human forearm, using magnets small enough for being implanted. The study proved the feasibility of tracking up to seven MMs randomly placed and moved within such workspace. To overcome this limit, in a more recent study we comprehensively searched for general rules useful to design systems dealing with multiple magnetic objectives, exploiting a planar configuration [15]. Specifically, in [15] we systematically analysed the effect of geometry and magnetization grade of the magnetic objectives, as well as the number of available sensors, on the localization accuracy. Nine to 18 magnets placed along a row were localized. The sensors were arranged on a rectangular grid. Results suggested that, irrespectively of the number of available sensors or the magnetization grade, an indefinite high number of magnets could be properly tracked, as long as a geometric design rule is respected [15]. Building on this, here, we sought to transfer such findings into a more realistic scenario, and to validate them by simulating the tracking of multiple magnets implanted in an anatomically appropriate model.

In a clinical scenario, the placement of the MMs would depend on the detailed geometry of the anatomy after the amputation, which is usually of traumatic nature [16]. As the performance of a magnetic tracking system strongly depends on its spatial features (i.e. the distance among MMs and between MMs and sensors [14], [15]), it is yet unknown how many magnets could fit in a residual forearm and be successfully tracked to restore independent control over multiple DoFs in a hand prosthesis. Thus, using a 3D CAD anatomical model of the forearm, we simulated the implant of n magnets in n available independent muscles. Specifically, we studied three representative amputation levels, in which residual limbs of different lengths hosted a different number of muscles/muscle portions. For each configuration, we defined both n and the implant sites based on the forearm anatomy and on the rules identified in our previous study [15]. A sensor selection strategy was also implemented in a way that, starting from an initial grid of $N = 840$ sensors, it identified a customized subset for each of the considered amputation levels. We simulated the displacement of the n magnets using a basic muscle model, and assessed the performance of the localizer by measuring its tracking accuracy.

Results showed that it is possible to track up to 11, 13 or 19 MMs using an array of 154, 205 and 260 sensors, in proximal, middle, or distal representative transradial amputations, respectively. We achieved remarkably accurate tracking performance, as localization errors always proved below 7% the trajectory of the MMs inside each muscle. These outcomes suggest that many magnets could be implanted and effectively tracked, thus allowing to achieve independent control of multiple DoFs in a hand prosthesis.

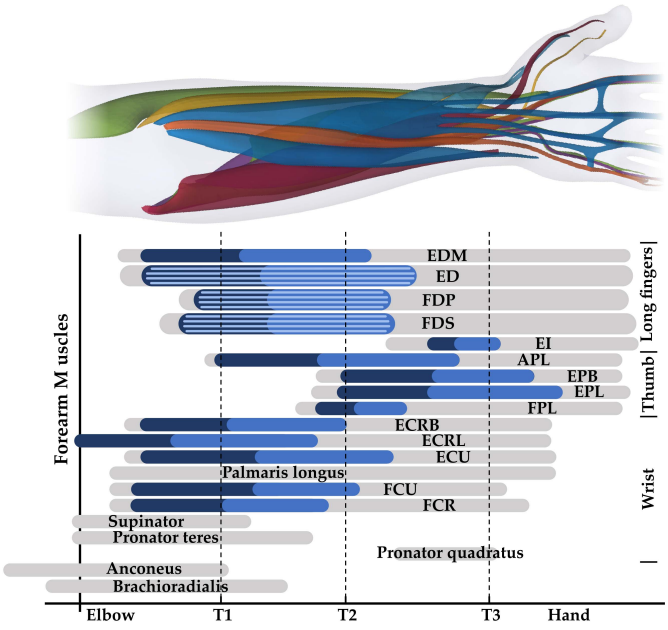

Fig. 1. Simulated amputation levels (T1, T2, T3) with respect to the anatomical distribution of the forearm muscles. The colored sections indicate the portions of the muscles considered suitable for the magnets implant. Specifically, dark blue sections refer to the muscle portions which are proximal to the aponeurosis insertion. Light blue lines indicate muscle compartments. Acronyms in Appendix.

II. Materials and Methods

We simulated three configurations resembling three possible levels of transradial amputation with the aid of a 3D CAD model of a healthy human forearm. This detailed bones, muscles, skin, and connective tissue (50^{th} percentile male; Zygote, American Fork, US, Fig. 1). The first and second configurations (T1 and T2) imitated amputations occurring at the first and second proximal third of the forearm, respectively. The third one (T3) accounted for an amputation across the carpal bones (wrist disarticulation) leaving most of the extrinsic hand muscles available for the implant (Fig. 1).

For each configuration, we first identified n, i.e. the number of magnets that could be implanted and tracked, and defined their position in the muscles. This was done through a *magnet placing procedure* that took into account: (i) the geometry of the residual forearm; (ii) a simplified biomechanical model of the muscle contraction; (iii) general guidelines identified in our previous study [15]. We then simulated the movements of the MMs caused by muscle contractions, and acquired their simulated magnetic field through N simulated sensors. Finally, we ran a localization algorithm to estimate the poses of the MMs based on the sensor readings, and verified the effectiveness of the placing procedure (we call this the *localization problem*).

A. Anatomical Constraints and Muscle Model

Almost all the muscles contained in the forearm, including each of the four compartments of the flexor digitorum profundus (FDP), superficialis (FDS) and extensor digitorum (ED)

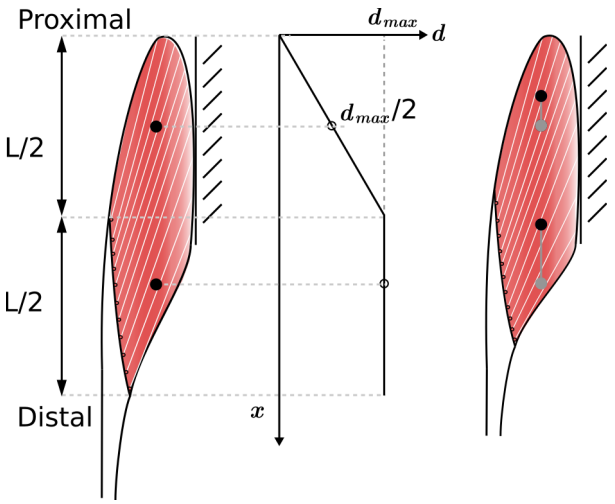

Fig. 2. Muscle contraction model. Left: relaxed muscle. Right: contracted muscle. During contraction, every point in the distal part of the muscle belly and of the distal aponeurosis move axially by d_{max}; every point in the proximal section moves axially proportionally to its distance from the muscle belly origin ($x = 0$). Radial displacements are neglected.

were considered as targets for the implant (Fig. 1). Few exceptions were the anconeus and the brachioradialis (which are not extrinsic hand muscles), the palmaris longus (absent in ∼15% of the population), the pronator teres, the pronator quadratus, and the supinator (Fig. 1). The latter were excluded because they only undergo a displacement when the radius and ulna bones are free to rotate relative to each other. However, prosthetic sockets usually prohibit this movement [17], making such muscles useless for the target application.

Only the muscles that after the simulated amputation exhibited bellies with a residual length of at least 20% the original one [16] were considered eligible for magnet implantation. According to such criterion, configuration T1, T2 and T3 presented a different number of eligible muscles/muscle compartments.

We modelled the displacement of the muscles, and thus of the implanted magnets, according to the following system of equations:

$$d(x) = \begin{cases} \dfrac{x}{L/2} d_{max}, & x < \dfrac{L}{2} \\ d_{max}, & x \geq \dfrac{L}{2} \end{cases} \quad (1)$$

where x is a coordinate lying on the curve that runs along the longitudinal axis of the muscle. The latter was defined as the third-degree polynomial fitting curve of the centroids of the available muscle (or muscle portion) cross-sections (0.3 mm step between sections) starting/ending at the ideal transition between the proximal/distal tendon and the belly. d_{max} is the maximum muscle contraction and L is the length of the muscle belly at rest (Fig. 2). This model, which roughly approximates the contraction of a pennate/bipennate muscle, is a simplification of more complex models available in the literature [18], [19]. In brief, when contracting, the distal part of the belly and the distal aponeurosis jointly move by an amount corresponding to d_{max}. The proximal section, instead, contracts proportionally to the distance from the muscle origin (Fig. 2).

The actual contractile ability of each muscle after the amputation surgery is generally unknown, as it depends on several anatomical, injury-related and recovery factors [16]. For this reason, we assumed a uniform d_{max} across all muscles, equal to 10 mm. Similarly, the length of the distal aponeurosis is highly variable across muscles, so this was set to L/2 (Fig. 2), in agreement with previous measurements of human pennate muscles [20], [21].

B. Magnets Placing Procedure

Magnets were modeled as Nd-Fe-B N45 grade cylindrical magnets (axial remanent magnetization $B_r = 1.27$ T, radius = 1 mm, height = 1 mm). A placing procedure was implemented for defining the initial (rest) position of the magnets in the residual muscles, for each configuration (i.e. T1, T2 and T3). Such procedure aimed at ensuring an accurate multi-magnet tracking by optimizing their arrangement in the anatomical space. It worked under the following hypotheses: (i) only one magnet could be implanted in each muscle/compartment; (ii) muscles deformation was assumed to take place only in the longitudinal direction, neglecting radial displacements; (iii) magnets could be implanted only in (sections of) the muscle belly, and not in the tendons; (iv) the magnetic moment vectors of the implanted MMs always pointed radially, in order to maximize the magnetic field measured by the sensors.

The placing procedure exploited a non-linear programming solver implemented in Matlab (*fmincon*, MathWorks, Natick, MA). Starting from some user-defined initial conditions, the solver follows a sequential quadratic programming method to iteratively converge to an optimal solution [22]. In this case, it searched for the placement that minimized the following cost function:

$$f(p) = -(1 + \overline{d_{MM}}) \sum_{i=1}^{n} R_i \quad (2)$$

with R_i:

$$R_i = \frac{L_{inter-MM_i}}{L_{MM-sensor_i}} \quad (3)$$

being a geometric parameter introduced in our previous work [15]. $L_{inter-MM_i}$ indicates the distance between the i-th MM and the nearest MM, and $L_{MM-sensor_i}$ is the distance between the ith MM and the nearest magnetic field sensor. $\overline{d_{MM}}$ is the modelled displacement of the muscle, normalized and averaged across all MMs. In mathematical terms, $\overline{d_{MM}} = \sum_{i=1}^{n} d_{MMi}/d_{max}$. p is a $3 \times n_k$ vector containing the coordinates of the n magnets at the kth iteration. Notably, in [15], we proved that the MMs with higher R values yielded to better localization accuracies.

The search space of the cost function was constrained by several factors: first, the MMs could only be placed in muscles sites eligible for the implant (i.e., in the centroids of the cross-sections of the available muscle); secondly, the spatial arrangement imposed $R_i \geq 0.6$ for each magnet, a condition

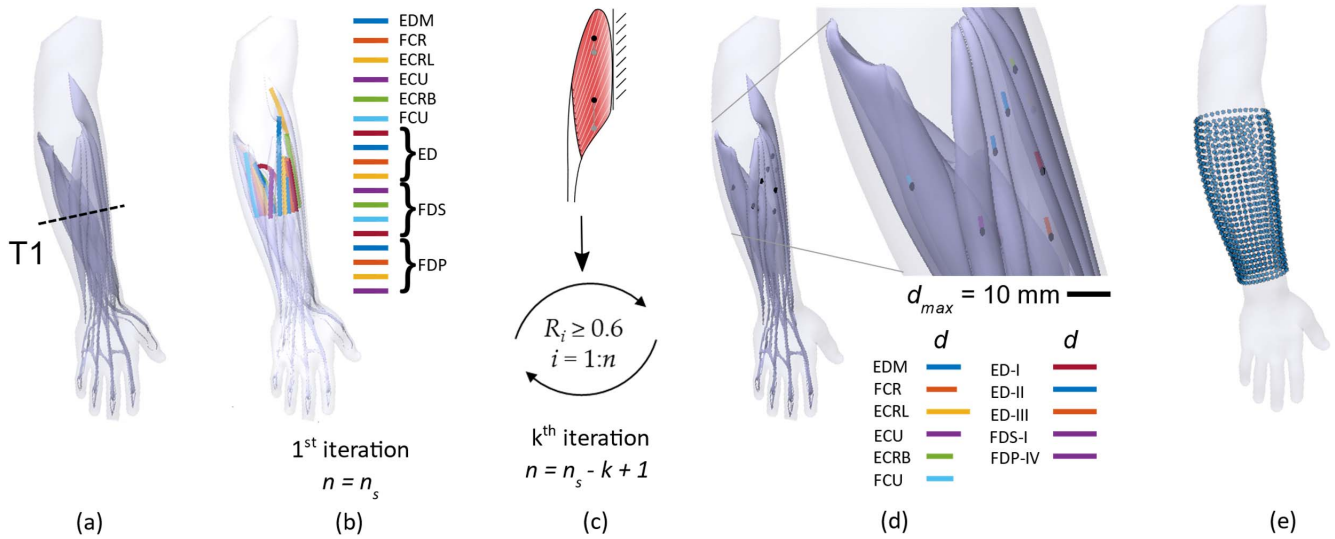

Fig. 3. Experimental methods. (a)-(d) Magnets placing procedure workflow. Once the amputation level is defined (e.g. T1) (a), the muscles eligible for the implant (n_S) are selected and their longitudinal axis is extracted from the 3D model (b). A non-linear programming solver iteratively places the magnets in the muscle axes until all of them *(n)* exhibit $R_i \geq 0.6$ (c) and optimal displacement of the trajectories, d (d). (e) Grid of N = 840 sensors placed around the forearm, starting approximately 1 cm below the elbow and ending 1 cm above the wrist.

supposed to ensure an accurate multi-magnet tracking [15]; thirdly, the shortest trajectory length of the MMs was set to be ~6 mm. To sum up, the procedure searched for a placement of the MMs that maximized both their R (Eq. 2 - 3) and displacement, in a space limited by the contraction trajectories.

The algorithm started by considering a number of MMs n_s equal to the number of muscles/compartments eligible for implantation. Then, after each iteration, the magnet that scored the lowest R (if below 0.6) was removed. The placing procedure was iterated until all $n_k \leq n_s$ MMs were successfully placed (all $R_i \geq 0.6$, Fig. 3a-d). In our earlier work, we proved that the MMs with higher R values yielded to better localization accuracies in the special case when both sensors and MMs are arranged on a plane [15]. Here we assessed if the same argument held true in a "refolded" and anatomically relevant workspace.

C. Localization Problem

Once the placing procedure was completed, the movements of the MMs were simulated, following anatomically appropriate trajectories along the muscle axis (Fig. 3d). Each trajectory originated in the site defined by the placing procedure, and ended proximally at a distance d_{MMi}. The displacement of the MMs was approximated by translating them, one at a time, along 11 equidistant checkpoints (0%, 10%, 20%, …, and 100% the trajectory length). At each checkpoint, we computed the magnetic field using an analytical model for a cylindrical magnet (described and validated earlier [23], [24]).

Such field was sampled on a grid of N simulated sensors arranged around the forearm, ideally hosted within a prosthetic socket. Specifically, the grid accounted for $N = 840$ sensors. The grid was shaped around the forearm 3D CAD model, starting approximately 1 cm below the elbow and ending approximately 1 cm above the wrist (Fig. 3e). The angular step for the grid, set to 12°, resulted in a distance between sensors between 5 mm and 14 mm ($L_{inter-sensor}$) along the circumference. Axially the $L_{inter-sensor}$ was set to 10 mm. All distances were compatible with the physical size of commercial Hall-effect sensors (MAG3110, NXP Semiconductors NV, Eindhoven, Netherlands).

Sensor recordings at each checkpoint were stored and subsequently fed to a Matlab script that ran the Levenberg-Marquardt algorithm [25] to retrieve the poses of the MMs offline. At the first checkpoint, the (compound) magnetic field was recorded across the whole sensor grid. Then, a sensor selection strategy (described in the next section) was implemented, aiming at reducing the computational complexity of the localization problem, while still ensuring adequate accuracy. Likewise, the algorithm approximated the MMs as point-like dipoles for solving the localization problem, akin to several previous works [12], [14].

The localization error, both in terms of position and orientation, was assessed relatively to the starting position as:

$$E_p \approx e_m + e_{ct} \tag{4}$$

where e_m accounts for inaccuracies in tracking the displacement of the moving magnet (i.e., model error), while e_{ct} accounts for false predictions of simultaneous displacement affecting the non-moving magnets (i.e., cross-talk effect). e_m and e_{ct} were defined as the Euclidean distance between the actual and the estimated displacement for the moving and non-moving MMs, respectively, akin to our previous works [10], [14], [15], [26].

D. Sensor Selection

Our previous work suggested the existence of a positive correlation between the localization accuracy and the distinguishability of the peaks in the magnetic field and its gradient [15]. Based on this idea we selected a subset of sensors for each configuration.

At the first checkpoint, a *calibration* was performed in which the (compound) magnetic field was recorded across the

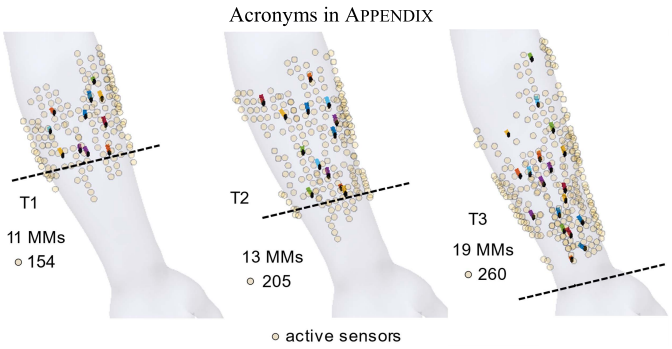

Fig. 4. Final placement of the magnets (black dots), associated trajectories (colored segments), and active sensors (yellow dots) following the placing and sensor selection procedures, for amputation levels T1, T2 and T3.

TABLE I
ELIGIBLE (E) AND SELECTED (S) MUSCLES FOR MMS IMPLANTATION

Muscle name	T1	T2	T3	Muscle name	T1	T2	T3
EDM	S	E	S	FDS-IV	E	S	S
ED-I	S	S	S	ECRB	S	S	S
ED-II	S	S	S	ECRL	S	S	S
ED-III	S	S	S	ECU	S	S	S
ED-IV	E	S	S	FCU	S	S	S
FDP-I	E	E	E	FCR	S	E	S
FDP-II	E	S	S	APL		E	S
FDP-III	E	S	S	FPL		S	S
FDP-IV	S	S	S	EI			S
FDS-I	S	E	S	EPB			E
FDS-II	E	E	E	EPL			S
FDS-III	E	E	E				

whole sensor grid ($N = 840$). The 2D gradient of both the radial and axial component of the magnetic field were then computed and the peaks in the field and in their gradients were identified through thresholding (thresholds set to 5 mG and 5 mG/$L_{inter-sensor}$, respectively; empirically set to ensure a trade-off between number of selected sensors and tracking accuracy). Finally, the sensors associated with at least one peak in either the magnetic field or its gradient were identified as the *active sensors*, and used to solve the localization problem across the whole simulation (i.e. for all checkpoints).

To validate this method, the localization accuracy obtained when using the set of active sensors was compared to that obtained when exploiting the whole grid.

III. RESULTS

Of the initial 18 (T1), 20 (T2) and 23 (T3) muscles eligible for implantation, the placing procedure selected 11, 13, and 19 to receive a MM (Fig. 4, Table I). More in detail, the procedure ensured a final $\overline{R}$ of 1.86 ± 0.72 for the shortest residual limb (T1), in which the implanted MMs could travel by an average displacement $\overline{d_{MM}}$ of 8.7 ± 1.7 mm. For the middle amputation level (T2), a final $\overline{R}$ of 2.21 ± 0.79, and $\overline{d_{MM}}$ of 9.3 ± 1.6 mm were obtained. Finally, in T3, the placing procedure led to a final $\overline{R}$ of 1.83 ± 0.68, with an average displacement $\overline{d_{MM}}$ of 9.3 ± 1.5 mm.

The proposed selection strategy identified a subset of 154 active sensors for configuration T1, 205 for T2 and 260 for T3 (Fig. 4). This corresponded to a reduction of ∼82 %, ∼76 % and ∼69 % the number of the initial grid and to a sensor-to-magnet ratio of 14, 15.8, and 13.7, respectively. The selected active sensors generally clustered around the regions surrounding the implanted magnets (Fig. 4).

For the sake of brevity, in the following we report the accuracy of the localization algorithm in retrieving the position of the MMs only. This because the error in estimating the orientations of the MMs proved always lower than 1°, and its trend closely matched with the position error. The results from a representative configuration (T1) are first presented (Fig. 5).

The relationship between the actual and the computed displacement proved always highly linear ($R^2 = 0.99$, $p < 0.001$, Fig. 5, upper panels), and the e_m demonstrated almost constant along the trajectory for all MMs. The latter ranged between <0.01 mm and 0.03 mm for all MMs except for the magnet implanted in FDP-IV (fourth compartment of the *flexor digitorum profundus*), for which it varied from 0.50 mm to 0.67 mm (minimum-maximum). Nevertheless, also in this case e_m proved always lower than 7% the trajectory covered by the magnet inside the hosting muscle. The movement of one MM affected the position estimate of the other MMs (Fig. 5, lower panels). The importance of this effect varied according to which MM was moved. Overall, e_{ct} proved always below 0.09 mm for all MMs except for the magnet in FDP-IV, for which a maximum e_{ct} of 0.31 mm was measured on its estimate while moving the magnet in ED-I (first compartment of the *extensor digitorum*) (Fig. 5, lower panels). This corresponded to 3% the trajectory length of the magnet inside the FDP-IV.

All in all, the errors demonstrated in the same order of magnitude when the residual limb length, and consequently the number of MMs, increased (configurations T2 and T3, Fig. 6). In particular, the largest e_m were obtained for the magnets in FDP-IV in configuration T2 ($e_m = 0.40$ mm), and in FDP-II in configuration T3 ($e_m = 0.15$ mm). The highest e_{ct} were 0.21 mm in configuration T2 and 0.27 mm in configuration T3, for the same magnets. Overall, e_m and e_{ct} proved always lower than 4% and 5% the displacement travelled by the MMs during muscle contraction.

The tracking accuracy obtained when acquiring the entire sensor grid and that obtained when using only the active sensors proved always comparable (Fig. 7). As a representative example, for the magnet in FDP-IV in T1 the maximum difference in e_m and e_{ct} proved equal to ∼0.39 mm and ∼0.24 mm, respectively (Fig. 7). The trends of the error in the two considered configurations, in terms of relative value across different MMs (muscles), closely matched (Fig. 7). Regarding configurations T2 and T3, a maximum difference of 0.21 mm and 0.11 mm for e_m, and of 0.12 mm and 0.24 mm for e_{ct} were obtained, respectively (not shown).

The localization accuracy generally worsened when R decreased (Fig. 8). Indeed, while no correlation was found for e_m (outlier value relative to FDP-IV excluded), a significant negative correlation was found for e_{ct} ($r = -0.69$, $p = 0.02$). Similar results for e_{ct} were found for configurations T2 ($r = -0.50$, $p = 0.08$) and T3 ($r = -0.52$, $p = 0.02$) (not shown). Although a perfect proportionality was not established

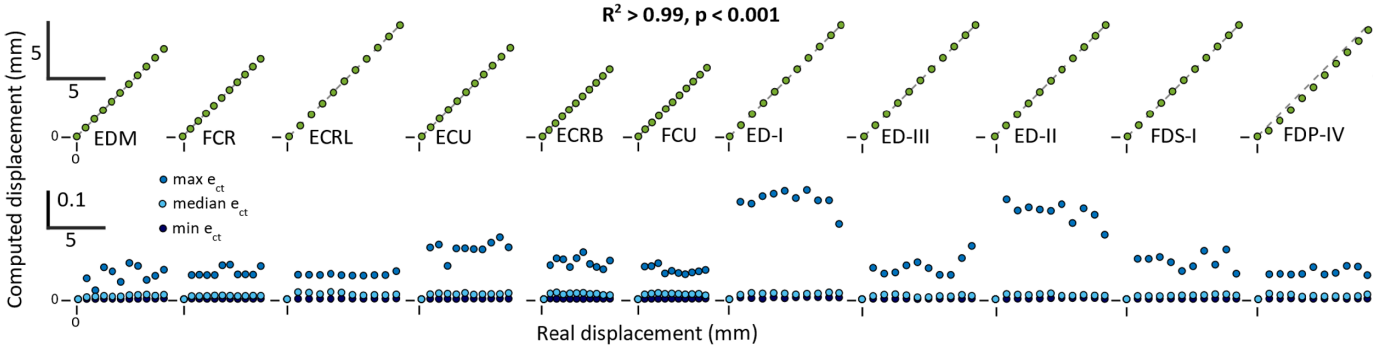

Fig. 5. Performance of the localizer in retrieving the displacement of the MMs in configuration T1 (using the selected active sensors). Each magnet was moved along a trajectory, while the remaining magnets were kept at their initial/rest position. The magnet implanted in FDP-IV showed the highest e_m and e_{ct}, respectively equal to 0.67 mm and 0.30 mm. Acronyms in APPENDIX.

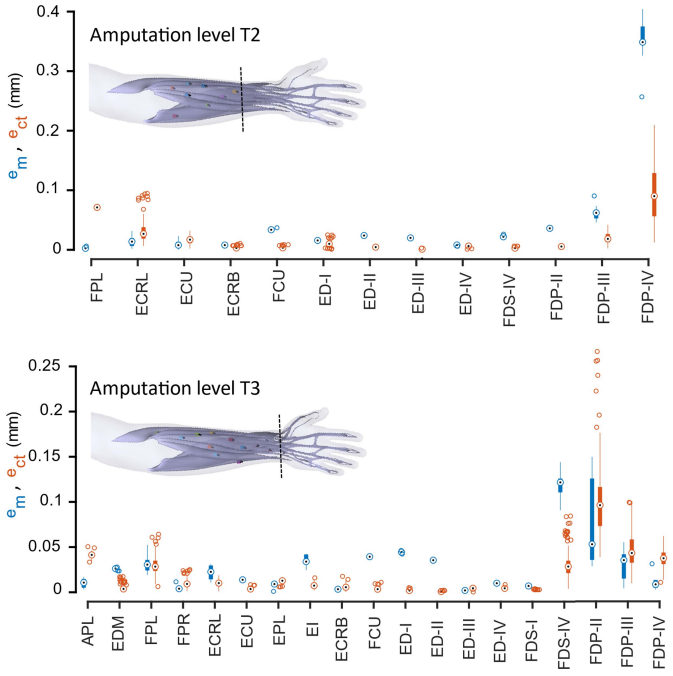

Fig. 6. Localization errors (e_m and e_{ct}) for configurations T2 and T3 (using the selected active sensors). The empty dots indicate the outliers, the boxplot encloses data within the interquartile range, the dot is the median value, while the whiskers extend to the limits of the distribution.

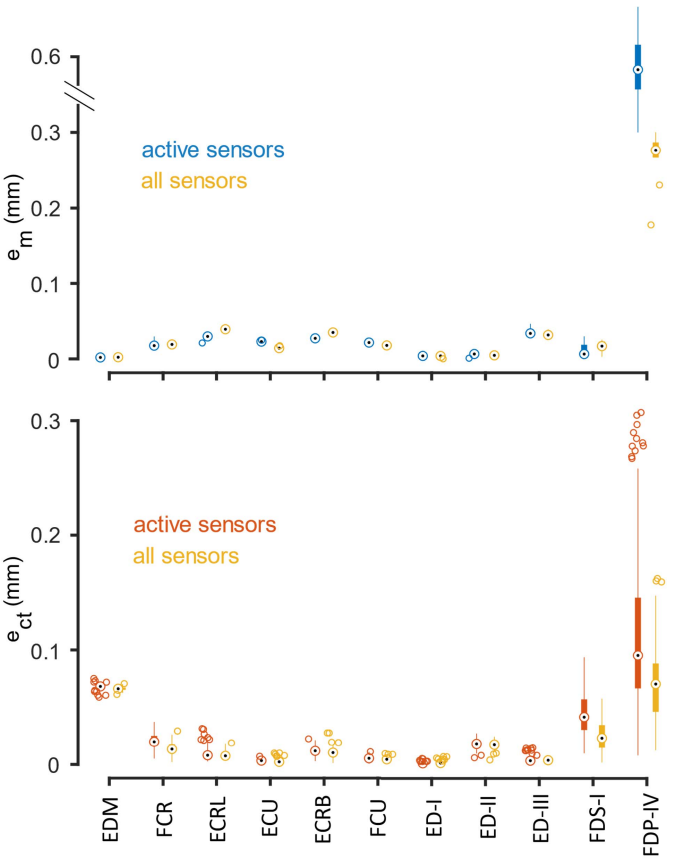

Fig. 7. Effect of the sensor selection on the localization errors (e_m and e_{ct}) for each magnet in configuration T1. The localization accuracy proved comparable when using the selected active sensors or all sensors.

between the accuracy and the R value, it is worth noticing that magnets in FDP-IV in configurations T1 and T2, and in FDP-II in configuration T3, showed both the highest e_m and the highest e_{ct}. At the same time, their R values proved largely below the average $\overline{R}$ measured for the corresponding configuration, and respectively equal to 0.76, 1.02 and 1.50.

IV. Discussion

In this work, we studied the effects of the complex anatomy of the human forearm on the design of a myokinetic interface aimed at controlling multiple DoFs of a hand prosthesis. Specifically, we hypothesized that by implanting MMs following specific geometrical constrains, we would be able to retrieve the position of several MMs with reasonable accuracy. As we indeed observed such performance, we conclude that our hypothesis was corroborated. To our knowledge, this is the first time that a localization algorithm is shown to successfully track such a large number of MMs, in simulation.

We could not find important differences in localization accuracy between the use of a uniform grid of sensors with respect to the ones selected (Fig. 7). This indicates that most of the information is retained after selection, supporting the idea that the localization accuracy of a magnet is related with the distinguishability of its peaks in the magnetic field (gradient). Notably, similar strategies to optimize the position and number of deployed sensors were already investigated in the literature, mostly for a single MM [12], [14], [27]–[29].

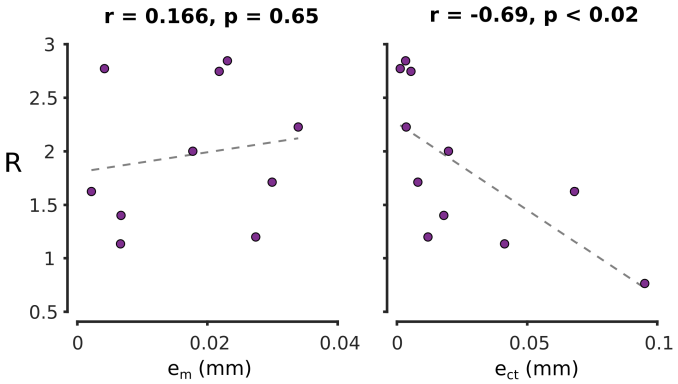

Fig. 8. Correlation between R and median e_m (left panel) or median e_{ct} (right panel) in configuration T1 (using the selected active sensors). While no correlation was found for e_m (outlier FDP-IV value excluded), a significant negative correlation was found for e_{ct}.

Regardless of the specific strategy, all of them agree on the need of 10-15 sensors per MM. Our method, by selecting 14-16 sensors/MM, aligns with the literature by extending the findings to systems with multiple MMs. Nonetheless, whether the distribution of sensors counts more than their number (as suggested by Maréchal and colleagues [27]) still remains to be assessed.

We found R to be inversely correlated with e_{ct} but not with e_m (Fig. 8). This finding seems in contrast with the argument brought by our previous study, in which we suggested a correlation between R and both e_m and e_{ct} [15]. However, we hypothesize that the absence of proportionality between R and e_m is caused by its very small range of values (maximum e_m below 0.04 mm), once removed the outlier exhibited by the magnet in FDP-IV.

Our previous study is the only one we are aware of dealing with multiple MMs (i.e., 18). In that study, however, we characterized a much simpler setup (featuring all MMs in a row) and exploited a virtually "infinite" number of sensors for their localization. Hence, this study supports but also considerably extends our previous findings. We show indeed that R is an appropriate metric also when dealing with complex distributions of MMs, each one being oriented in a different direction, and using a reduced number of sensors.

Although we applied our methodologies to the anatomy of a healthy human forearm, this approach could be readily translated in clinical settings. Indeed, the muscles distribution of a specific patient could be provided by advanced 3D MRI-based techniques [30]–[33]. As an example, Diffusion-Tensor MRI was shown to provide a detailed reconstruction and segmentation of single forearm muscles [30]. By planning the placement of the MMs in advance, we could significantly reduce the duration of the surgical procedure and, at the same time, optimize the performance of the prosthesis control system. On the other hand, we introduced a few simplifications in the analysis. First, we hypothesized that all muscles and muscle compartments could be contracted independently. However, it is known that neural and mechanical connections coupling inter and intra-muscle contractions exist in humans [34], [35]. Secondly, we considered that a muscle after amputation deforms similarly to muscles in unaffected forearms. In fact, there is clinical evidence that residual muscles spontaneously tend to stick to the surrounding tissue. Furthermore, during the amputation surgery, it is common practice to suture the muscle directly to the bone (myodesis) or together with other muscles (myoplasty), in order to prevent pain at the residual limb [36]. It remains to be demonstrated if any surgical procedure (e.g. a regenerative agonist-antagonist myoneural interface - AMI - [37]) could mitigate such drawbacks.

Even if MMs could potentially be implanted in different sites of the muscle (e.g., the muscle surface or the tendon), we selected the muscle belly because we expect it to have a reduced sensitivity to external deformations (e.g., pushing on the skin) [38]. In turn, this should improve the robustness of the control system during clinical use. Allowing to implant the MMs also on distal tendons, would have surely affected $L_{inter-MM}$, allowing for larger Rs.

We assumed the distal aponeurosis to insert in the muscle L/2 far from the muscle origin, for all muscles. Although this represented a simplification, it is worth noticing that, while the effective insertion of the aponeurosis affects the actual displacement of the muscle (and of the MM), it does not affect the placement of the implanted magnet. Furthermore, as the aponeurosis could be intentionally slackened/adjusted during the amputation surgery, it would not be possible to identify a precise value for each muscle which is accurate in general.

The present study was indeed limited in some respects. First, in order to limit the number of combinations tested, we fixed the orientation of the MMs to point towards the sensors. This is the optimal configuration, selected to maximize the magnetic field sampled by the sensors. However, we expect variability in the orientation of the MMs during the manual implantation in the muscles, which should be considered in the simulation. Secondly, mechanical disturbances (e.g. the weight of the prosthesis itself, collisions with the environment) could generate relative displacements between the muscles and the sensors, affecting the localization performance. Corrective actions (e.g. using a fixed magnet) should be investigated in order to mitigate such drawback. Thirdly, we considered a simplified linear model to describe the muscle contraction. This only captured axial deformations, while it is known that muscles deform radially as well. Finally, the simplified model was applied without modification to all forearm muscles, not reflecting differences in muscle contractile properties. A more realistic model would greatly affect how MMs move and should thus be considered in future studies. Additionally, the whole study is based on computer simulations. Although experimental validation is always beneficial, we compared simulated and experimental setups in early studies. This was performed for both a planar [15] and an anatomically relevant [10] workspace. We think these studies already adequately support the translatability of the results presented here to the physical world. Finally, the placing procedure selected muscles without considering their function, or their mapping with the available DoFs in a prosthesis. Thus, it may be interesting to associate importance indexes to muscles so that those with pivotal functions would be retained more easily.

In conclusion, we demonstrated for the first time the feasibility of tracking several MMs with a very good accuracy. Up to 19 MMs could be tracked in a realistic volume,

resembling the anatomy of the limb. While further investigations are still required to assess the transferability of the findings to a real-world scenario and to allow for proper comparison with alternative advanced methods [3], [6], [9], we argue that this work represents an important step forward for the development of an intuitive control system for multi-fingered hand prostheses. Not least, these outcomes are of great interests for a multitude of biomedical applications that exploit multi-magnet tracking in a constrained workspace.

APPENDIX

EDM – extensor digiti minimi. ED – extensor digitorum. FDP – flexor digitorum profundus. FDS – flexor digitorum superficialis. EI – extensor indicis. APL – abductor pollicis longus. EPB – extensor pollicis brevis. EPL - extensor pollicis longus. FPL – flexor pollicis longus. ECRB – extensor carpi radialis brevis. ECRL – extensor carpi radialis longus. ECU - extensor carpi ulnaris. FCU – flexor carpi ulnaris. FCR – flexor carpi radialis.

REFERENCES

[1] S. Amsuess, P. Goebel, B. Graimann, and D. Farina, "Extending mode switching to multiple degrees of freedom in hand prosthesis control is not efficient," in *Proc. 36th Annu. Int. Conf. IEEE Eng. Med. Biol. Soc. (EMBC)*, Aug. 2014, pp. 658–661.

[2] R. F. Weir, P. R. Troyk, G. A. DeMichele, D. A. Kerns, J. F. Schorsch, and H. Maas, "Implantable myoelectric sensors (IMESs) for intramuscular electromyogram recording," *IEEE Trans. Biomed. Eng.*, vol. 56, no. 1, pp. 159–171, Jan. 2009.

[3] P. F. Pasquina *et al.*, "First-in-man demonstration of a fully implanted myoelectric sensors system to control an advanced electromechanical prosthetic hand," *J. Neurosci. Methods*, vol. 244, pp. 85–93, Apr. 2015.

[4] M. Ortiz-Catalan, B. Hakansson, and R. Branemark, "An osseointegrated human-machine gateway for long-term sensory feedback and motor control of artificial limbs," *Sci. Transl. Med.*, vol. 6, no. 257, p. 257re6, Oct. 2014.

[5] *DeTOP Project*. Accessed: Mar. 23, 2020. [Online]. Available: http://www.detop-project.eu/

[6] T. A. Kuiken *et al.*, "Targeted muscle reinnervation for real-time myoelectric control of multifunction artificial arms," *J. Amer. Med. Assoc.*, vol. 301, no. 6, pp. 619–628, 2009.

[7] M. G. Urbanchek *et al.*, "Development of a regenerative peripheral nerve interface for control of a neuroprosthetic limb," *BioMed Res. Int.*, vol. 2016, pp. 1–8, Oct. 2016.

[8] P. P. Vu *et al.*, "A regenerative peripheral nerve interface allows real-time control of an artificial hand in upper limb amputees," *Sci. Transl. Med.*, vol. 12, no. 533, Mar. 2020, Art. no. eaay2857.

[9] J. M. Hahne, M. A. Schweisfurth, M. Koppe, and D. Farina, "Simultaneous control of multiple functions of bionic hand prostheses: Performance and robustness in end users," *Sci. Robot.*, vol. 3, no. 19, Jun. 2018, Art. no. eaat3630.

[10] S. Tarantino, F. Clemente, D. Barone, M. Controzzi, and C. Cipriani, "The myokinetic control interface: Tracking implanted magnets as a means for prosthetic control," *Sci. Rep.*, vol. 7, no. 1, Dec. 2017, Art. no. 17149.

[11] A. M. Franz, T. Haidegger, W. Birkfellner, K. Cleary, T. M. Peters, and L. Maier-Hein, "Electromagnetic tracking in medicine—A review of technology, validation, and applications," *IEEE Trans. Med. Imag.*, vol. 33, no. 8, pp. 1702–1725, Aug. 2014.

[12] W. Yang, C. Hu, M. Li, M. Q.-H. Meng, and S. Song, "A new tracking system for three magnetic objectives," *IEEE Trans. Magn.*, vol. 46, no. 12, pp. 4023–4029, Dec. 2010.

[13] C. R. Taylor, H. G. Abramson, and H. M. Herr, "Low-latency tracking of multiple permanent magnets," *IEEE Sensors J.*, vol. 19, no. 23, pp. 11458–11468, Dec. 2019.

[14] S. Tarantino, F. Clemente, A. De Simone, and C. Cipriani, "Feasibility of tracking multiple implanted magnets with a myokinetic control interface: Simulation and experimental evidence based on the point dipole model," *IEEE Trans. Biomed. Eng.*, vol. 67, no. 5, pp. 1282–1292, May 2020.

[15] M. Gherardini, F. Clemente, S. Milici, and C. Cipriani, "Localization accuracy of multiple magnets in a myokinetic control interface," *Sci. Rep.*, submitted for publication.

[16] D. F. Fisher, "Atlas of amputations and limb deficiencies: Surgical, prosthetic, and rehabilitation principles," *J. Vascular Surg.*, vol. 42, no. 6, p. 1246, Dec. 2005.

[17] I. Boni, J. Millenaar, M. Controzzi, and M. Ortiz-Catalan, "Restoring natural forearm rotation in transradial osseointegrated amputees," *IEEE Trans. Neural Syst. Rehabil. Eng.*, vol. 26, no. 12, pp. 2333–2341, Dec. 2018.

[18] B. A. Garner and M. G. Pandy, "Estimation of musculotendon properties in the human upper limb," *Ann. Biomed. Eng.*, vol. 31, no. 2, pp. 207–220, Feb. 2003.

[19] Z. Li, J. P. M. Mogk, D. Lee, J. Bibliowicz, and A. M. Agur, "Development of an architecturally comprehensive database of forearm flexors and extensors from a single cadaveric specimen," *Comput. Methods Biomech. Biomed. Eng., Imag. Vis.*, vol. 3, no. 1, pp. 3–12, Jan. 2015.

[20] T. Muramatsu, T. Muraoka, D. Takeshita, Y. Kawakami, and T. Fukunaga, "*In vivo* mechanical properties of proximal and distal aponeuroses in human tibialis anterior muscle," *Cells Tissues Organs*, vol. 170, nos. 2–3, pp. 162–169, 2002.

[21] T. Muramatsu, T. Muraoka, Y. Kawakami, and T. Fukunaga, "Superficial aponeurosis of human gastrocnemius is elongated during contraction: Implications for modeling muscle-tendon unit," *J. Biomech.*, vol. 35, no. 2, pp. 217–223, Feb. 2002.

[22] H. E. Romeijn, F. Schoen, and A. Fallis, *Handbook of Global Optimization*. Boston, MA, USA: Springer, 1995.

[23] N. Derby and S. Olbert, "Cylindrical magnets and ideal solenoids," *Amer. J. Phys.*, vol. 78, no. 3, pp. 229–235, Mar. 2010.

[24] A. Caciagli, R. J. Baars, A. P. Philipse, and B. W. M. Kuipers, "Exact expression for the magnetic field of a finite cylinder with arbitrary uniform magnetization," *J. Magn. Magn. Mater.*, vol. 456, pp. 423–432, Jun. 2018.

[25] J. J. Moré, "The Levenberg-Marquardt algorithm: Implementation and theory," in *Numerical Analysis*. Berlin, Germany: Springer, 1978.

[26] F. Clemente, V. Ianniciello, M. Gherardini, and C. Cipriani, "Development of an embedded myokinetic prosthetic hand controller," *Sensors*, vol. 19, no. 14, p. 3137, Jul. 2019.

[27] L. Maréchal, S. Foong, S. Ding, K. L. Wood, V. Patil, and R. Gupta, "Design optimization of a magnetic field-based localization device for enhanced ventriculostomy," *J. Med. Devices*, vol. 10, no. 1, pp. 1–9, Mar. 2016.

[28] S. Song, X. Qiu, J. Wang, and M. Q.-H. Meng, "Design and optimization strategy of sensor array layout for magnetic localization system," *IEEE Sensors J.*, vol. 17, no. 6, pp. 1849–1857, Mar. 2017.

[29] O. Talcoth and T. Rylander, "Optimization of sensor positions in magnetic tracking," Dept. Signals Syst., Chalmers Univ. Technol., Göteborg, Sweden, Tech. Rep. R015/2011, 2011.

[30] M. Froeling *et al.*, "Diffusion-tensor MRI reveals the complex muscle architecture of the human forearm," *J. Magn. Reson. Imag.*, vol. 36, no. 1, pp. 237–248, Jul. 2012.

[31] J. Su, H. Zou, and T. Guo, "The study of mechanical properties on soft tissue of human forearm *in vivo*," in *Proc. 3rd Int. Conf. Bioinf. Biomed. Eng. (iCBBE)*, Jun. 2009, pp. 1–4.

[32] B. Gilles, L. Moccozet, and N. Magnenat-Thalmann, "Anatomical modelling of the musculoskeletal system from MRI," in *Medical Image Computing and Computer-Assisted Intervention*. Berlin, Germany: Springer, 2006, pp. 289–296.

[33] C. M. Eng, G. D. Abrams, L. R. Smallwood, R. L. Lieber, and S. R. Ward, "Forearm muscle volumes can be accurately quantified from high resolution magnetic resonance imaging (MRI)," *J. Biomech.*, vol. 40, no. 14, pp. 3261–3266, 2007.

[34] S. L. Kilbreath and S. C. Gandevia, "Limited independent flexion of the thumb and fingers in human subjects," *J. Physiol.*, vol. 479, no. 3, pp. 487–497, Sep. 1994.

[35] C. Cipriani, J. L. Segil, J. A. Birdwell, and R. F. F. Weir, "Dexterous control of a prosthetic hand using fine-wire intramuscular electrodes in targeted extrinsic muscles," *IEEE Trans. Neural Syst. Rehabil. Eng.*, vol. 22, no. 4, pp. 828–836, Jul. 2014.

[36] S. Ovadia and M. Askari, "Upper extremity amputations and prosthetics," *Seminars Plastic Surg.*, vol. 29, no. 1, pp. 55–61, Feb. 2015.

[37] S. S. Srinivasan, M. Diaz, M. Carty, and H. M. Herr, "Towards functional restoration for persons with limb amputation: A dual-stage implementation of regenerative agonist-antagonist myoneural interfaces," *Sci. Rep.*, vol. 9, no. 1, Dec. 2019, Art. no. 1981.

[38] G. T. Yamaguchi, *Dynamic Modeling of Musculoskeletal Motion*. Boston, MA, USA: Springer, 2001.